ARCHIVIO ISTITUZIONALE
DELLA RICERCA

Alma Mater Studiorum Università di Bologna
Archivio istituzionale della ricerca

A method to design biomimetic scaffolds for bone tissue engineering based on Voronoi lattices

This is the submitted version (pre peer-review, preprint) of the following publication:

Published Version:
A method to design biomimetic scaffolds for bone tissue engineering based on Voronoi lattices / Fantini, M; Curto, M.; De Crescenzio, F.. - In: VIRTUAL AND PHYSICAL PROTOTYPING. - ISSN 1745-2759. - STAMPA. - 11:2(2016), pp. 77-90. [10.1080/17452759.2016.1172301]

Availability:
This version is available at: https://hdl.handle.net/11585/569826 since: 2016-11-23

Published:

DOI: http://doi.org/10.1080/17452759.2016.1172301

Terms of use:

Some rights reserved. The terms and conditions for the reuse of this version of the manuscript are specified in the publishing policy. For all terms of use and more information see the publisher's website.

This item was downloaded from IRIS Università di Bologna (https://cris.unibo.it/).
When citing, please refer to the published version.

(Article begins on next page)

24 April 2024

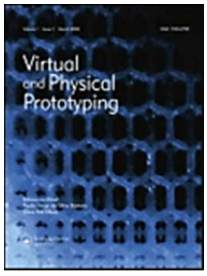

A method to design biomimetic scaffolds for Bone Tissue Engineering based on Voronoi lattices

Journal:	*Virtual and Physical Prototyping*
Manuscript ID	NVPP-2016-0008.R2
Manuscript Type:	Original Article
Keywords:	3d Scaffolds, Voronoi Diagram, Generative Design

SCHOLARONE™
Manuscripts

For Peer Review Only

A method to design biomimetic scaffolds for Bone Tissue Engineering based on Voronoi lattices

KEYWORDS: 3d Scaffolds, Voronoi Diagram, Generative Design

For Peer Review Only

Abstract

In regenerative medicine, 3D scaffolds are used to sustain the regeneration of tissues in removed or damaged parts of the human body. As such practices are being widely experimented in clinical applications, the design, the materials and the manufacturing process to obtain efficient 3D biocompatible lattices are being significantly investigated. Nevertheless, most of the proposed designs are based on regular 3D shapes obtained from the repetition of unit cells disposed in a three-dimensional array. This approach does not exploit the whole potential of Computer Aided Design tools coupled with manufacturing capabilities for freeform shapes. In this paper, we propose a method to model biomimetic lattices controlling the porosity and the pores size of scaffolds to be integrated with the anatomical shape of the defect. The method has been implemented in bone tissue case study and implements a Generative Design approach based on Voronoi diagrams.

1. Introduction

Designing synthetic scaffolds for guided tissue regeneration is a very challenging issue. The primary function of a scaffold is to provide a structural template that serves to bear loads of the surrounding tissues, while the cells progressively regenerate in the scaffold volume (Chevallay and Herbage 2000; Yang et al. 2001; Hollister 2005; Saxena 2005). The success of the scaffold depends on several factors which are related to the form of the lattice and to the material used to manufacture it (Ramakrishna et al. 2001; Dee, Puleo and Bizios 2002; Molly and Stevens 2008; Shrivats, McDermott and Hollinger 2014).

On the form side, the requirements that need to be met can be classified into two main levels: i) the external boundary surface of the scaffold must be coherent with the anatomy of the patient to be replaced; ii) the internal porous and interconnected

microstructure of the scaffold must favor the cells proliferation in the entire volume to be regenerated. Therefore, the scaffold must reproduce the shape of the tissue graft and the ingrowth of cells needs a trabecular architecture, in which the percentage porosity and the pores size must be controllable (Hollister et al. 2000; Wettergreen et al. 2005; Van Cleynenbreugel et al. 2006). These features of the scaffold, together with the degree of pores interconnection (or interconnectivity), have impact on the time and quality of the regeneration (Williams et al. 2006).

Generally, for bone scaffolds, the pores size should be maintained in a given range [150 μm ÷ 600 μm] (Cornell 1999) and the porosity of the bone can differ according tothe specific bone site considered. In literature, it is reported that the bone trabecular morphology is a porous environment variable in a range between ~~[~~50% ~~÷~~ and 90%~~]~~ whereas the compact bone tissue has a lower porosity [<10%] (Hollister and Kikuchi 1994; Salgado, Coutinho and Reis 2004) due to the *Haversian channels*.

On the material side, the ideal material should be biocompatible and biodegradable, in order to allow the total replacement of biological tissue once the regeneration of tissues is completed (Hollinger and Wong 1996).

Customized porous scaffolds can be obtained by Subtractive Manufacturing (Ciocca et al. 2013a; Ciocca et al. 2013b), starting from blocks of porous material manufactured by different technologies through conventional fabrication methods, including techniques such as solvent casting and particulate leaching, gas foaming, fiber meshes and fiber bonding, phase separation, melt molding, emulsion freeze drying, solution casting and freeze drying (Sachlos and Czernuszka 2003). Also, customized porous scaffolds can be directly manufactured by means of advanced fabrication methods, such as Solid Freeform Fabrication (SFF) or Additive Manufacturing (AM) (Naing et al. 2005; Quadrani et al. 2008; Abdelaal and Darwish 2011)of biocompatible and biodegradable materials.

Several limitations are related to the conventional fabrication methods. These are mainly concerned with the precise control of the pores size, followed by pores geometry, pores interconnection, spatial distribution of pores and construction of internal channels within the scaffold (Peltola et al. 2008). Through Additive Manufacturing, on the other hand, it is virtually possible to control the internal morphology of the scaffold. Limitations concerned with the 3D printed scaffolds are due to material inhomogeneity, limited choice of materials, minimum resolution and

For Peer Review Only

accuracy of machines and, in some cases, difficulty in removing the support material in very deep and small pores (Hollister, Maddox and Taboas 2002).

For what concerns the biomedical field, Additive Manufacturing has been widely used for the production of customized surgical guides, bone plates and anatomical prosthesis (Ciocca et al. 2011; Dobbe et al. 2011; Ciocca et al. 2012; Mazzoli 2013). Recently, advances in Additive Manufacturing are also opening the way to a better employment of this technology for the production of customized scaffolds and for the CAD modeling of anatomic and porous structures to be printed in 3D.

A modern approach to scaffold design is based on the use of hierarchical structures created by the repetition of a unit cell of known geometry and known properties and on the possibility to predict the properties of the scaffolds since the properties of the unit cell are known. A variety of geometries and geometry libraries have been proposed and their geometrical and mechanical properties have been compared and reported (Hoffmann and Arinyo 2002; Chua et al. 2003; Sun et al 2005; Bucklen et al 2008; Gabbrielli, Turner and Bowen 2008). However, the unit cell approach produces trabecular architectures that do not really mimic the morphology of porous skeletal structures. These geometries are mainly based on a Constructive Solid Geometry (CSG) approach and reflect, once combined with the 3D model of the bone graft substitute, a scarcely natural appearance.

To overcome this limitation, we propose a method to create customized biomimetic internal scaffolds with a porous and interconnected microstructure, as it appears in natural bone, based on a Generative Design approach. Since Generative Design is not about designing a shape, but it is about designing the process that builds a shape, this approach allows the user to obtain complex shapes by an automatic modeling process, and to customize the results by interactively modifying certain parameters.

The proposed method starts with the generation of Voronoi diagrams. Starting from a discrete number of points called seeds, a Voronoi diagram is the result of a specific space partition in which every cell is composed of the points that are closer to the generating seed. Voronoi diagrams received and receive so much attention because of their presence in nature and they are being exploited for the generation of shapes in different fields, such as architecture, jewelry and industrial design in general.

The paper is organized as follows. The next section gives information on the Voronoi diagrams and on the way they work. Afterward, the workflow for the generation of a

For Peer Review Only

Voronoi-based lattice is described. Results and the way for controlling the features parameters are discussed in the last section before the conclusions.

2. Methods: Generation of biomimetic scaffolds based on Voronoi lattice

2.1. Voronoi Diagram

Since its introduction and practical application in the early 20th century, the Voronoi diagram, initially described by Dirichlet (1850) and Voronoi (1908), has been a popular topic not only in computational geometry ~~and~~ but also in a variety of disciplines. Many natural processes can be used to define particular classes of Voronoi diagrams. Since they are related to several well-known geometrical structures, various authors believe that the Voronoi diagram is one of the most fundamental constructs defined by a discrete set of points. Therefore, such diagrams have increasingly attracted the attention of researchers and computer scientists in the last few years (Aurenhammer 1991).

The ordinary Voronoi diagram, for a point set and its construction, has been studied extensively in both two and higher dimensions (Okabea, Bootsb and Sugihara 1994). In a 2D vector space, where the Voronoi diagram is modeled, points, lines and polygons are primitives. The primitives, in higher dimensions, are built upon the lower dimensionality primitives. In our case, for the third dimension, we consider the polyhedrons. The Voronoi theory can be thought of as below (Van der Putte and Using 2009).

Let the finite Euclidean space contain a certain number (n) of points (with $n > 1$), called seeds. Around each seed a circle is drawn, with a starting radius of 0, expanding at the same rate until two circles touch so that a line or boundary is formed. The circles keep expanding until they cannot expand any further (Fig. 1). The resulting graph is the Voronoi diagram for that set of points. The diagram is built corresponding to the areas in which each point location is closest to the seed corresponding to that area.

Fig. 1 Graphical representation about the formation of a 2D Voronoi diagram

For Peer Review Only

The mathematical equation of such a polygon $V(p_i)$ can be expressed as follows (Okabe, Boots and Sugihara 1992):

$$V(p_i) = \{ p/d(p, p_i) \leq d(p, p_j), j \neq i , j = 1, \dots , n \}$$

Where:

- $p_1, \dots , p_n$ *is* a set of distinct seeds located in R^d
- $d(p, p_i)$ represents the Euclidean distance between location p and seed p_i
- $V(p_i)$ represents the ordinary Voronoi polygon associated with seed p_i

In 2D, Voronoi cells are separated from each other by boundaries that consist of line segments. The Voronoi cell consists of a convex polygon without holes. In 3D, these boundaries consist of planes, and the cells consist of convex polyhedrons without holes. In Fig. 2, an example of the 3D Voronoi diagram is shown.

Fig.2 a) Reference cube, b) 3D Voronoi polyhedron, c) Partition in 3D Voronoi polyhedrons

2.2. Voronoi-based lattice generation

In this section, a Generative Design workflow implementing the 3D Voronoi diagram for modeling bone tissue engineering scaffolds is proposed (Fig. 3). The aim is to automatically build a trabecular structure, starting from a set of points randomly distributed in the bounding box volume of the bone defective part to be replaced, hereafter called patient bone geometry. This process allows to obtain a customized scaffold controlling the percentage porosity and pores size in order to reach the desired values.

Fig. 3 Workflow for the 3D Voronoi scaffold generation

The generative workflow allows to design a porous and interconnected lattice ready to be 3D printed, starting from a data set of four inputs: the patient bone geometry acquired from CT scan and surgery planning, the number of seeds (n) and two scale factors (S_f and S_v). The output is generated through a series of sub-routines

For Peer Review Only

implemented in sub-circuits designed in Grasshopper, the graphical algorithm editor integrated into Rhinoceros 5. The first sub-circuit works on the bounding box of the patient bone geometry, creating a set of points randomly distributed in the bounding box volume (*Populate 3D*). Such points will be the seeds to generate the 3D Voronoi structure that divides the bounding box volume into a set of polyhedral cells (Fig. 4). Each cell, being a closed polysurface, encloses a volume and each face of the cell coincides with the boundary face of the adjacent cell. With the aim to gather a porous and interconnected lattice structure, we need to generate a single closed polysurface, namely a solid, with the seeds at the center of the pores and void channels to interconnect these pores.

Fig. 4 Partition in Voronoi polyhedrons of the bounding box volume generated from the patient anatomy

The method here described is based on the idea of building the lattice as a network of solid beams along the edges of the polyhedral cells generated above. Starting from these polyhedrons, a deconstruction operation (*DeBrep*) is applied in order to obtain the boundary representation of each polyhedral cell, in terms of a list of faces, edges and vertices (F, E, V). Thus, the *DeBrep* component allows the separation of all the faces from the 3D Voronoi diagram. Two parallel computations are then performed. The first one starts from the faces of the polyhedral cells and scales each face assuming its centroid as reference point with a scale factor S_f. In parallel, each starting polyhedral cell is scaled assuming its centroid as reference point with a scale factor S_v. (Fig. 5).

Fig. 5 a) Each face is scaled respect the face's centroid, b) each polyhedron is scaled respect the polyhedron's centroid

Next, the faces, edges and vertices of such smaller polyhedral cells are obtained again through the *DeBrep* component. Hence, we have the edges of the scaled faces of the starting cells and the edges of the faces of the scaled cells. These edges are the skeleton of the trabecular structure. Then, in order to obtain the beams of the

For Peer Review Only

trabeculae we need to build a solid on these edges. This is done by generating a series of quad meshes on the edges vertex, which can be extracted in the proper list (Fig. 6).

Fig. 6 a) Generation and deconstruction of faces and polyhedrons, b) particular of scaled feces and polyhedrons, c) quad meshes on the edges to construct the lattice

Before the final intersection for producing the customized scaffold, there is another component that makes an essential task, based on the *Catmull-Clark* algorithm. This is a technique used in computer graphics to create smooth surfaces by subdivision surface modeling. Edwin Catmull and Jim Clark devised it in 1978 as a generalization of bi-cubic uniform B-spline surfaces to arbitrary topology. By this component, which is contained in the Rhinos plug-in Wavebird for shape reconstructing, a smoothed lattice mesh can be obtained (Fig. 7).

Fig. 7 a) Trabecular mesh, b) Smoothed lattice mesh after *Catmull-Clark* algorithm

Finally, a mesh Boolean intersection is performed between the patient bone geometry mesh and the Voronoi lattice mesh in order to obtain the customized scaffold mesh of the bone graft (Fig. 8).

Fig. 8 Boolean intersection of the patient bone geometry and the lattices to obtain the porous scaffold

It is clear that varying the number of seeds (n) and the scale factor for the faces (S_f) and for the volume (S_v) of the polyhedral cells into a range from [0÷1], a different lattice is obtained in terms of percentage porosity and pores size. In order to find the correlation between these input parameters (number of seeds and scale factors) and the target parameters (percentage porosity and pores size), in the next section, an analysis procedure is proposed. It is based on comparing the key parameters for the scaffold evaluation such as percentage porosity, pores size, pores interconnection and trabecular thickness.

3. Results

For Peer Review Only

In order to control the final trabecular morphology of the porous and interconnected Voronoi scaffold, we need to correlate the input parameters with the target ones. The input parameters are:

- the number of seeds (n) to be included in the bounding box of the scaffold;
- the scale factors S_f and S_v.

The target parameters that we consider in this paper are:

- the percentage porosity P%;
- the pores size.

The percentage porosity P% can be easily computed as follows:

$$P\% = \frac{V_{bounding\ box} - V_{scaffold}}{V_{bounding\ box}} \times 100$$

Since:

$$V_{void} = V_{bounding\ box} - V_{scaffold}$$

Actually, we can show how the number of seeds and the scale factors S_f and S_v influence the percentage porosity, where:

- S_f is the polyhedrons faces scale factor;
- S_v is the polyhedrons volume scale factor.

First of all, by varying each scale factor in a range of [0÷1] and maintaining the same number of seeds, we derived a sample of scaffold and measured the percentage porosity (P%), which is referred to each pair of values of the two scale factors. In Fig. 9 three snapshots of a cubic scaffold (10×10×10 mm), with the same number of seeds (n = 500), generated by setting $S_f = S_v = 0.25$ for the first one, $S_f = S_v = 0.50$ for the second one and $S_f = S_v = 0.75$ for the third one, are depicted.

Fig. 9 Sample of scaffold (10×10×10 mm) with 500 seeds and setting: a) $S_f = S_v = 0.25$ (P% = 17.4), b) $S_f = S_v = 0.50$ (P% = 47.8), c) $S_f = S_v = 0.75$ (P% = 79.6)

Afterward, we plotted the percentage porosity obtained by varying the S_v scale factor for different values of the S_f scale factor. Results are shown in Fig. 10.

Fig. 10 Effect of the scale factors Sf and Sv on the percentage porosity of the lattice (with 500 seeds)

For Peer Review Only

Then, for each pair of values of the two scale factors (S_f and S_v), we generated a sample of scaffold by varying the number of seeds in a range of [100÷1000], with incremental steps of 50, and computed the percentage porosity (P%). Results are shown in Fig. 11 for the sample of scaffold generated by setting $S_f = S_v = 0.75$.

Fig. 11 Effect of the number of seeds on the percentage porosity of the scaffold (with Sf= Sv = 0.75)

The first observation on these results concerns the impact of the number of seeds onto the percentage porosity. By varying the number of seeds, we can observe that the variation in the percentage porosity of the scaffolds in a sample, characterized by constant values of S_f and S_v, is very low. This can be explained considering that the number of seeds determines both the number of pores and the number of trabeculae at the same time. Thus, a larger number of seeds means a larger number of pores (voids), but also a larger number of trabeculae (solids), whose presence balances the total amount of the void volume. Therefore, it can be assumed that the scale factors S_f and S_v are related to the expected percentage porosity (P%) of the final scaffold with a very low influence of the number of seeds (n): the greater are the scale factors the higher is the total porosity. To obtain, for example, an expected percentage porosity P% ≈ 80%, both scale factors (S_f and S_v) have to be set to 0.75. Of course, the geometries of the scaffolds will differ for different combinations of S_f and S_v that allow obtaining the same value of percentage porosity.

Since for a given combination of S_f and S_v we can control the porosity with a good accuracy, we can now observe the effect of a different number of seeds (n) on the morphology of the scaffold.

The number of seeds (or the seeds density as the number of seed points per unit volume) can be given in order to gather a target pores size of the scaffold. Hence, this is a significant parameter that has to be identified and quantified being also an important index for cells habitability. The ideal populating input number of seeds can be estimated in relation to the target percentage porosity and the target pores size, by setting the relative desired values as input.

To this aim, starting from the bounding box volume of the scaffold, the total void volume can be easily estimated as a function of the target percentage porosity (P%). Assuming that all the pores have a spherical shape with the same diameter (D_p), the

For Peer Review Only

total number of pores is computed as the target total void volume subdivided by the volume of a single sphere of the given diameter.

By the proposed workflow for the 3D Voronoi scaffold generation, the pores (voids) can be represented by the polyhedral cells and, therefore, the number of pores corresponds to the number of seeds.

In this way, the ideal populating input number of seeds (n) is estimated as the ratio of the target total void volume and the volume of the sphere with the diameter (D_p) representing the target pores size.

$$n = \frac{V_{bounding\ box} \times P\%}{\frac{4}{3}\pi\left(\frac{D_p}{2}\right)^3}$$

Since:

$$V_{void} = V_{bounding\ box} \times P\%$$

Then, to evaluate the actual size of the randomly created pores, we propose the following method. Since the pores have ~~not a~~ irregular shapes, the idea is based on the identification, for each polyhedron, of the sphere that is centered at the centroid of the polyhedral cell and has the same volume of the polyhedron scaled by S_v. This will be recalled as the polyhedron-sphere method. In Fig. 12 the approximated spherical pores are depicted for a sample of scaffold with the shape of a cube 10 mm sided (P% = 81.6 and 100 seeds). In this way, we can evaluate the size of each pore as the diameter of the related polyhedron-sphere, so that a comparison with the literature values, included between [150 µm ÷ 600 µm] can be provided, starting from the number of seeds set as input in the Voronoi diagram.

Fig. 12 Polyhedron-sphere method: a) polyhedrons scaled by S_v, b) polyhedrons scaled by S_v and corresponding spheres, c) spheres representing the pores

Therefore, we generated a sample of scaffold (10×10×10 mm), with a bounding box volume = 1000 mm^3, setting $S_f = S_v = 0.75$ to obtain an expected percentage porosity P% ≈ 80%. The number of Voronoi seeds was estimated in relation to target percentage porosity (P% = 80%) and the target pores size (varying from 5.00 mm to 0.50 mm), as the ratio of the target total void volume (800 mm^3) to the volume of the sphere with the diameter representing the target pores size (Fig. 13).

For Peer Review Only

Fig. 13 Number of Voronoi seeds estimated in relation to the target pores size for a cubic scaffold 10 mm sided with a target percentage porosity P% = 80%

Then, the actual outcoming size of each pore of the scaffold, generated with different target pores size (and, therefore, different number of seeds), was measured by applying the polyhedron-sphere method. The results are reported in Fig. 14.

Fig. 14 Pores size (measured applying the polyhedron-sphere method) of a cubic scaffold 10 mm sided, scale factors Sf = Sv = 0.75, with a target percentage porosity P% = 80%, generated with different target pores size (and therefore different number of seeds)

In Fig. 15 two snapshots of a cubic scaffold 10 mm sided, with the same scale factors ($S_f = S_v = 0.75$), generated with a different number of seeds (200, 800), are depicted.

Fig. 15 Sample of scaffold (10x10x10 mm) with $S_f = S_v = 0.75$ and setting: a) number of seeds = 200 (target pores size = 2 mm), b) number of seeds = 800 (target pores size = 1 mm)

The first observation on these results shows as the number of Voronoi seeds rapidly increases with the decreasing of the target pores size: in the sample of scaffold with the shape of a cube 10 mm sided, a target pores size of 5 mm corresponds to 12 seeds, while a target pores size of 0.5 mm correspond to 12'223 seeds. To obtain, for example, the actual size of each pore included in the range [150 μm ÷ 600 μm], a suitable target pores size can be set to 0.6 or 0.5 mm.

The second observation concerns the size of the actual pores that is almost entirely smaller than the target one. Since on the generated scaffold the pores have different dimensions, their measures can slightly differ from the target value. We observed that in the generated scaffold the maximum pores size approximate with a good accuracy the target pores size, and the variance is relatively low, remaining below 1 and decreasing with the increasing of the number of seeds. This can be explained considering that the total pores void, computed by the polyhedron-sphere method, results, as expected, in 421.875 mm^3, since the starting Voronoi polyhedrons (with total volume 1000 mm^3) are scaled by S_v = 0.75 in the 3 dimensions (1000 $mm^3 \times 0.75 \times 0.75 \times 0.75$ = 421.875 mm^3). The remaining part of void (378,125 mm^3) to reach the expected 80% porosity (800 mm^3) is due to connective channels between the pores, essential to assure a correct pores interconnection.

For Peer Review Only

Moreover, the number of seeds can give us information about the number of pores inside the customized scaffold. Since the input is given as the number of points to be included in the bounding box of the patient bone geometry, we initially assumed that the number of seeds in the model of the customized scaffold depends on the ratio between the volume of this model and the volume of its bounding box. Therefore, a rough estimation of the number of seeds (and, therefore, pores) in the final scaffold can be based on this proportion. Actually, depending on the shape of the patient bone geometry, a different number of expected seeds (and therefore pores) can be included in the final mesh of the customized scaffold.

Another key parameter for the scaffold evaluation is the pores interconnection (or interconnectivity) that is the property, which allows the perfusion of nutrients and the extrusion of wasting material inside the cancellous bone structure. This is the main reason for preferring scaffolds with a high permeability structure that also ensures the availability of higher surface area for enhanced cell adhesion and proliferation. Therefore, the degree of pores interconnection can be considered as important as ~~the~~ pores size.

In the case of the generated Voronoi scaffold, we tried to understand how each pore communicates with its neighbors, and in particular to find the number and the size of the connective channels departing from each pore.

We have already seen that the pores (voids) can be represented by the polyhedral cells scaled by S_v and that the actual size of the pores can be evaluated by means of the polyhedron-sphere method.

If we look at the void component (pores plus connective channels) of a very simple cubic Voronoi scaffold (10 mm sided), generated with only 8 seeds corresponding to the bounding box vertices and minimal scale factors ($S_f = S_v = 0.25$), we can observe how the 8 pores are mutually interconnected (Fig. 16a).

Fig. 16 Void component (pores plus connective channels) for a Voronoi scaffold with minimal scale factors (Sf = Sv = 0.25) and a) number of seeds = 8, b) number of seeds = 9

For each of the 8 polyhedrons (that are cubes in this case), six connective channels depart, one from each face of the cube, giving the impression that the resulting structure is six-fold connected. If we add another seed (the centroid of the bounding box), we can now observe 9 polyhedral cells with different shapes and more faces with respect to the previous case (Fig. 16b). Since the connective channels are still

For Peer Review Only

departing from each face of the polyhedrons to run out to the corresponding face of the neighbor, the level of interconnectivity increases with the number of Voronoi seeds. Moreover, we can also observe that the size of each connective channel is represented by the area of the departing face of the polyhedral cell.

Therefore, we can conclude that the mean number of faces of the polyhedrons could give the level of interconnectivity of the generated Voronoi scaffold, and the mean area of the faces of the polyhedrons could give the mean size of the connective channels. The properties of the connective channels have been computed as the mean pores interconnection and mean channels size for a Voronoi scaffold with a target percentage porosity (P% = 80%) and varying the target pores size (from 5.00 mm to 0.50 mm), as depicted in Fig. 17.

Fig. 17 Mean pores interconnection and mean channels size of a cubic scaffold 10 mm sided, scale factors Sf = Sv = 0.75, with a target percentage porosity P% = 80%, generated with different target pores size (and therefore different number of seeds)

Finally, the trabecular thickness (that represents the solid part of the scaffold opposite to the total void volume) can be evaluated as the mean value of the distance between the centroids of the coupled faces of neighboring polyhedral cells scaled by S_v. We have seen that Voronoi polyhedrons, scaled by S_v, can represent the pores (voids) of the scaffold structure, evaluated by means of the polyhedron-sphere method, therefore, the trabecular skeleton is built up in the free space between these cells (Fig. 18).

Fig. 18 Trabecular thickness evaluation: a) Voronoi polyhedral cells scaled by Sv with the distance of the centroids of coupled faces; b) Voronoi polyhedral cells scaled by Sv with the trabecular mesh; c) the final scaffold (Sf = Sv = 0.75; number of seeds n = 12; target pores size D_p= 5 mm)

The trabecular thickness has been computed for a Voronoi scaffold with a target percentage porosity (P% = 80%) and by varying the target pores size (from 5.00 mm to 0.50 mm), as depicted in Fig. 19.

Fig. 19 Mean pores interconnection and mean channels size of a cubic scaffold 10 mm sided, scale factors Sf = Sv = 0.75, with a target percentage porosity P% = 80%, generated with different target pores size (and therefore different number of seeds)

4. Discussion

The main findings of this work concern two aspects, which are the general design method and the CAD approach followed. The general design method resulted very

For Peer Review Only

efficient since the generation of biomimetic porous lattices, shaped on the patient anatomy, is very intuitive and fast. Moreover, great accuracy in the expected percentage porosity and pores size has been achieved by setting the suitable input parameters. The CAD approach also resulted positive since a closed and watertight mesh of the customized porous scaffold, for different bone grafts, have been obtained in a short time. This allows to directly interfacing the generative modeling module for the generation of porous interconnected scaffolds with Additive Manufacturing systems.

These findings can be explained by the fact that the interactive Generative Design approach, which has been developed from Voronoi diagram, is independent by the final shape of the scaffold and allows to simply modify the input parameters in suitable ranges for satisfying the surgical requirements in terms of both percentage porosity and pores size.

In a recent review about the design of scaffold for bone tissue engineering, considering the emergence of Solid Freeform Fabrication (SFF) methods (Velasco, Narváez-Tovar and Garzón-Alvarado 2015), the main reported design techniques, in previous relevant works, are based on Constructive Solid Geometry (CSG), Boundary Representation (B-Rep) and, in the last years, on implicit surfaces like Triply Periodic Minimal Surfaces (TPMS). Only a case study based on Voronoi diagrams for general irregular porous structures modeling has been reported (Kou and Tan 2010). However, this paper does not investigate key parameters for bone replacement scaffolds generation, such as percentage porosity, pores size, pores interconnection and trabecular thickness. Moreover, no practical recommendations are provided for guiding the design of internal trabecular morphology of the bone scaffold.

Furthermore, the new and important aspect of this study is not the design of a specific scaffold, but the development of a general interactive method to design different customized scaffolds according to the specific requirements provided by the clinical team. Therefore, the proposed method can be a useful tool for the design of biomimetic scaffolds for bone regeneration.

Nevertheless, together with the design, ~~also~~ materials and manufacturing processes also play ~~a~~ fundamental roles in obtaining~~to obtain~~ efficient 3D biocompatible scaffolds with this internal trabecular microstructure. For this reason, the capabilities of Additive Manufacturing, according to the biomaterials used, should allow the

For Peer Review Only

manufacturability of these scaffolds in terms of percentage porosity, pores size, pores interconnection and trabecular thickness.

Additive Manufacturing is evolving from rapid prototyping to the end-of-use product manufacturing and offers numerous benefits for innovative design solutions. Nowadays, design freedom has been significantly broadened, including shape complexity, material complexity, hierarchical complexity, and functional complexity (Gibson, Rosen and Stucker 2010; Yang and Zhao 2015).

The emerging field of Design for Additive Manufacturing (DFAM) is exploring new methodological frameworks and design rules, but is also highlighting geometrical limitations and constraints to be considered (Adam and Zimmer 2015; Kumke, Watschke and Vietor 2016).

Therefore, to validate the manufacturability of the proposed biomimetic scaffolds based on Voronoi diagram, a review of possible methods that can be used in the actual fabrication, in terms of Additive Manufacturing systems and biomaterials, is reported. The three main classes of synthetic biomaterials used today are metals, ceramics and polymers.

The class of biomaterials with a long history of application in bone implants comprises of metals and alloys. Among them, the use of stainless steels, cobalt (Co), titanium (Ti) and relative alloys are well proven due to their good biocompatibility, satisfactory mechanical strength and superior corrosion resistance. Therefore, Metal-based Additive Manufacturing (MAM) techniques, such as Selective Laser Melting (SLM) and Electron Beam Melting (EBM), are increasingly being used for the fabrication of porous metals for bone scaffolds and orthopaedic implants, with predefined external shape and internal architecture (Wang et al. 2016).

For example, Yan et al. (2015) reported that Ti-6Al-4V biomorphic lattices for bone implants were manufactured by Selective Laser Melting (SLM). The design was based on Gyroid and Diamond Triply Periodic Minimal Surface (TPMS), having an interconnected high porosity of 80-95% and pores size in the range of 560-1600 μm and 480-1450 μm respectively. The manufacturability, microstructure and mechanical properties were evaluated and the comparison between 3D micro-CT reconstructed models and original CAD models of the Ti-6Al-4V TPMS lattices showed excellent reproduction of the designs.

Also, Taniguchi et al. (2016) studied the effect of pores size on bone ingrowth into porous titanium implants fabricated by Selective Laser Melting (SLM), since this

For Peer Review Only

Additive Manufacturing technique has the ability to produce metallic scaffolds with accurately controlled porosity, pores size and interconnectivity for orthopedic applications. Three porous titanium implants, based on a Diamond lattice basic structure (with an intended porosity of 65% and pores size of 300, 600, and 900 μm,), were successfully manufactured by EOSINT-M270 SLM system. The porous implants were evaluated using Computed Tomography and the actual average pores size resulted of 309, 632, and 956 μm, respectively.

Finally, Sing et al. (2015) investigated the effect of design and process parameters on the dimensional accuracy of titanium lattice structures fabricated by using Selective Laser Melting (SLM). Geometrical design parameters, such as unit cell type and strut diameter, had not significant effects on the dimensional accuracy of the lattice structures. On the other hand, the processing parameters, such as laser power and laser scan speed, had a significant effect on the powder adhesion on the struts and consequentially affected the dimensional accuracy.

In the field of ceramic biomaterials, Sabree et al. (2015) reported on how highly porous ceramic scaffolds have been fabricated by using stereolithography and the lost-mould process combined with gel-casting. All scaffolds had a simple cubic strut structure with an internal porosity of approximately 42% and internal pore dimensions in the range of 300-600 μm.

For what concerns the class of polymers as biomaterials, another method for the actual fabrication of Voronoi-based lattices could be the manufacturing as Poly(propylene fumarate) (PPF) scaffolds by using an EnvisionTEC Perfactory 3D Printer. Poly(propylene fumarate) is an important biodegradable and crosslinkable polymer designed for bone tissue-engineering applications. EnvisionTEC Perfactory 3D Printer is a rapid prototyping manufacturing system, based on Digital Light Processing (DLP) technology, to create 3D models that range from the conceptual to the fully functional. Some examples of fabrication of porous PPF scaffolds, as a huge opportunity for the regenerative medicine, have been proposed.

Wang et al. (2015) reported the manufacturing of porous, cylindrical scaffolds, consisting of modular ring-shaped bases, with 500 μm wall thickness, two pore sizes (400 μm and 800 μm) and two different porosities (25% and 50%). More recently, Luo et al. (2016) have described the fabrication of a porous, cylindrical scaffold, by using the Schoen Gyroid Triply Periodic Minimal Surface (TPMS) geometry, with 400 μm strut thickness, pore diameter of 1400 μm, and porosity of 88.2%.

For Peer Review Only

Actually, the next step of this work will be the concrete fabrication of the proposed Voronoi-based lattices to directly assess the manufacturability. Moreover, as a natural extension of this work could aim to find a proper seeds distribution to allow the generation of scaffolds with non-homogenous porosity, for example, with higher density for the compact external part (cortical or compact bone tissue) and lower density for the trabecular internal one (cancellous or spongy bone tissue). Since the initial distribution of Voronoi seeds influences the final scaffold trabecular morphology, non-homogenous scaffolds could be obtained with a higher concentration of seeds distribution in the external part and lower in the internal one. This method can be also refined and/or expanded on other requirements, such as the mechanical properties, once the density of seeds has been related to such properties.

However, some limitations of this study should be also considered, since a drawback of this approach is related to the generation of very large scaffolds due to the computational resources required.

5. Conclusions

In this paper, we proposed a method to design interconnected porous lattices that mimic specific tissue characteristics for the realization of bone regenerative scaffolds. The shape of reference is a healthy spongy bone, which presents a heterogeneous structure to enhance the cells proliferation and the tissue regeneration. The greater advantage of this method, compared to other approaches, is to provide geometrical heterogeneity thus resulting in a really biomimetic shape (Fig. 20).

The method is applied to provide an intuitive and fast tool to create biomimetic scaffolds and is expandable to other tissue engineering requirements or to other domains in which the design porous interconnected structures is needed.

Fig. 20 a) 3D generated Voronoi Scaffold, b) Healthy spongy bone (Marinozzi et al. 2012)

For Peer Review Only

References

Abdelaal OA, Darwish SM. Fabrication of Tissue Engineering Scaffolds Using Rapid Prototyping Techniques. World Academy of Science, Engineering and Technology. 2011;59:11-27.

Adam GAO, Zimmer D. On design for additive manufacturing: evaluating geometrical limitations Rapid Prototyping J. 2015;21(6):662-670.

Aurenhammer F. Voronoi diagrams – A survey of a Fundamental Geometric Data Structure. AMC Computing Surveys. 1991;23(3):345-405.

Bucklen BS, Wettergreen MA, Yuksel E, Liebschner MAK. Bone-derived CAD Library for Assembly of Scaffolds in Computer-Aided Tissue Engineering. Virtual Phys Prototyp. 2008;3(1):13-23.

Chevallay B, Herbage D. Collagen-based biomaterials as 3D scaffold for cell cultures: applications for tissue engineering and gene therapy. Med Biol Eng Comput. 2000;38(2):211-218.

Chua CK, Leong KF, Cheah CM, Chua SW. Development of a Tissue Engineering Scaffold Structure Library for Rapid Prototyping. Part 1: Investigation and Classification. Int J Adv Manuf Technol. 2003;21:291-301.

Ciocca L, Fantini M, De Crescenzio F, Corinaldesi G, Scotti R. Direct metal laser sintering (DMLS) of a customized titanium mesh for prosthetically guided bone regeneration of atrophic maxillary arches. Med Biol Eng Comput. 2011;49(11):1347-1352.

Ciocca L, Mazzoni S, Fantini M, Persiani F, Baldissara P, Marchetti C, Scotti R. A CAD/CAM-prototyped anatomical condylar prosthesis connected to a custom-made bone plate to support a fibula free flap. Med Biol Eng Comput. 2012;50(7):743-749.

For Peer Review Only

Ciocca L, Donati D, Ragazzini S, Dozza B, Rossi F, Fantini M, Spadari A, Romagnoli N, Landi E, Tampieri A, Piattelli A, Iezzi G, Scotti R. Mesenchymal Stem Cells and Platelet Gel Improve Bone Deposition within CAD-CAM Custom-Made Ceramic HA Scaffolds for Condyle Substitution. Biomed Res Int. 2013; Article ID 549762, 10 pages.

Ciocca L, Donati D, Fantini M, Landi E, Piattelli A, Iezzi G, Tampieri A, Spadari A, Romagnoli N, Scotti R. CAD-CAM generated hydroxyapatite scaffold to replace the mandibular condyle in sheep: preliminary results. J Biomater Appl. 2013;28(2):207-218.

Cornell CN. Osteoconductive materials and their role as substitutes for autogenous bone grafts. Orthopedic Clinics of North America. 1999;30(4):591-598.

Dee KC, Puleo DA, Bizios R. An Introduction to Tissue-Biomaterial Interaction. John Wiley & Sons. 2002;3:37-52.

Dobbe JDD, Vroemen JC, Strackee SD, Streekstra GJ. Patient-tailored plate for bone fixation and accurate 3D positioning in corrective osteotomy. Med Biol Eng Comput. 2011;51(1):19-27.

Gabbrielli R, Turner IG, Bowen CR, Development of Modelling Methods for Materials to be Used as Bone Substitutes. Key Engineering Materials. 2008;361-363:903-906.

Gibson I, Rosen DW, Stucker B. Additive Manufacturing technologies: rapid prototyping to direct digital manufacturing. 2010, Springer, US.

Hoffmann C, Arinyo RJ. Parametric Modelling. Handbook of CAGD, Farin G, Hoschek J, Kim MS, eds. Elsevier. 2002;519-541.

Hollinger J, Wong ME. The integrated processes of hard tissue regeneration with special emphasis on fracture healing. Oral Surg Oral Med Oral Pathol Oral Radiol Endod. 1996;82(6);595-606.

For Peer Review Only

Hollister SJ. Porous scaffold design for tissue engineering. Nat Mater. 2005;4(7):518-524.

Hollister SJ, Kikuchi N. Homogenization Theory and Digital Imaging: A Basis for Studying the Mechanics and Design Principles of Bone Tissue. Biotechnology and Bioengineering. 1994;43(7):586-596.

Hollister SJ, Maddox RD, Taboas JM. Optimal design and fabrication of scaffolds to mimic tissue properties and satisfy biological constraints. Biomaterials. 2002;23:4095-4103.

Hollister SJ, Levy RA, Chu TM, Halloran JW, Feinberg SE. An image based approach for designing and manufacturing craniofacial scaffolds. Int J Oral Maxillofac Surg. 2000;29(1):67-71.

Kou XY, Tan ST. A simple and effective geometric representation for irregular porous structure modelling. Comput Aided Des. 2010;42(10): 930-941.

Kumke M, Watschke H, Vietor T. A new methodological framework for design for additive manufacturing. Virtual Phys Prototyp. 2016;11(1):3-19.

Luo Y, Dolder CK, Walker JM, Mishra R, Dean D, Becker ML. Synthesis and Biological Evaluation of Well-Defined Poly(propylene fumarate) Oligomers and Their Use in 3D Printed Scaffolds. Biomacromolecules. 2016;17(2):690-697.

Marinozzi F, Marinozzi A, Bini F, Zuppante F, Pecci R, Bedini R. Variability of morphometric parameters of human trabecular tissue from coxo-arthritis and osteoporotic samples. Ann Ist Super Sanita. 2012;48(1):19-25.

Mazzoli A. Selective laser sintering in biomedical engineering. Med Biol Eng Comput. 2013;51(3):245-256.

For Peer Review Only

Molly M, Stevens MM. Biomaterials for bone tissue engineering. Materials Today. 2008;11(5):18-25.

Naing MW, Chua CK, Leong KF, Wang Y. Fabrication of customised scaffolds using computer-aided design and rapid prototyping techniques. Rapid Prototyping J. 2005;11(4):249-259.

Okabe A, Boots B, Sugihara K. Spatial Tessellations - Concepts and Applications of Voronoi Diagrams. Wiley, 1992.

Okabea A, Bootsb B, Sugiharac K. Nearest neighbourhood operations with generalized Voronoi diagrams: a review. Int J Geogr Inf Sci. 1994;8(1):43-71.

Peltola SM, Melchels FP, Grijpma DW, Kellomäki M. A review of rapid prototyping techniques for tissue engineering purposes. Ann Med. 2008;40(4):268-280.

Quadrani P, Pasini A, X Mattioli-Belmonte M, Zannoni C, Tampieri A, Landi E, Giantomassi F, Natali D, Casali F, Biagini G, Tomei-Minardi A. High-resolution 3D scaffold model for engineered tissue fabrication using a rapid prototyping technique. Med Biol Eng Comput 2005;43(2):196-199.

Ramakrishna S, Mayer J, Wintermantel E, Leong KW. Biomedical applications of polymer-composite materials: a review. Compos Sci Technol. 2001;61:1189-1224.

Sabree I, Gough JE, Derby B. Mechanical properties of porous ceramic scaffolds: Influence of internal dimensions. Ceramics International. 2015;(41):8425-8432.

Sachlos E, Czernuszka JT. Making tissue engineering scaffolds work. Review on the application of solid freeform fabrication technology to the production of tissue engineering scaffolds. Eur Cell Mater. 2003;5:29-40.

Salgado AJ, Coutinho OP, Reis RL. Bone Tissue Engineering: State of the Art and Future Trends. Macromol Biosci. 2004;4(8):743-765.

For Peer Review Only

Saxena AK. Tissue engineering: Present concepts and strategies. J Indian Assoc Pediatr Surg. 2005;10:14-19.

Shrivats AR, McDermott MC, Hollinger JO. Bone tissue engineering: state of the union. Drug Discov Today. 2014;19(6):781-786.

Sing SL, Yeong WY, Wiria FE, Tay BY. (2015) Characterization of Titanium Lattice Structures Fabricated by Selective Laser Melting Using an Adapted Compressive Test Method. Experimental Mechanics. Advance online publication. DOI 10.1007/s11340-015-0117-y.

Sun W, Starly B, Nam J, Darling A. Bio-CAD modelling and its applications in computer-aided tissue engineering. Comput Aided Des. 2005;37:1097-1114.

Taniguchi N, Fujibayashi S, Takemoto M, Sasaki K, Otsuki B, Nakamura T, Matsushita T, Kokubo T, Matsuda S. Effect of pore size on bone ingrowth into porous titanium implants fabricated by additive manufacturing: An in vivo experiment. Mater Sci Eng C Mater Biol Appl. 2016;59:690-701.

Van Cleynenbreugel T, Schrooten J, Van Oosterwyck H, Vander Sloten J. Micro-CT-based screening of biomechanical and structural properties of bone tissue engineering scaffolds. Med Biol Eng Comput. 2006;44(7):517-525.

Van der Putte, T. Using the discrete 3D Voronoi diagram for the modelling of 3D continuous information in geosciences. Master Thesis, Geographical Information Management and Applications. Utrecht University, Netherlands, 2009.

Velasco MA, Narváez-Tovar CA, Garzón-Alvarado DA. Design, Materials, and Mechanobiology of Biodegradable Scaffolds for Bone Tissue Engineering. Biomed Res Int. 2015, Article ID 729076, 21 pages.

Wang MO, Vorwald CE, Dreher ML, Mott EJ, Cheng MH, Cinar A, Mehdizadeh H, Somo S, Dean D, Brey EM, Fisher JP. Evaluating 3D-printed biomaterials as scaffolds for vascularized bone tissue engineering. Adv Mater. 2015;27(1):138-144.

For Peer Review Only

Wang X, Xu S, Zhou S, Xu W, Leary M, Choong P, Qian M, Brandt M, Xie YM. Topological design and additive manufacturing of porous metals for bone scaffolds and orthopaedic implants: A review. Biomaterials. 2016;83:127-141.

Wettergreen MA, Bucklen BS, Sun W, Liebschner MAK. Computer-Aided Tissue Engineering of a Human Vertebral Body. Ann Biomed Eng. 2005;33(10):1333-1343.

Williams JM, Adewunmi A, Schek RM, Flanagan CL, Krebsbach PH, Feinberg SE, Hollister SJ, Das S. Bone tissue engineering using polycaprolactone scaffolds fabricated via selective laser sintering. Biomaterials. 2005;26(23):4817-4827.

Yan C, Hao L, Hussein A, Young P. Ti-6Al-4V triply periodic minimal surface structures for bone implants fabricated via selective laser melting. J Mech Behav Biomed Mater. 2015;51:61-73.

Yang S, Leong KF, Du Z, Chua CK. The Design of Scaffolds for Use in Tissue Engineering. Part I Traditional Factors. Tissue Eng. 2001;7(6):679-689.

Yang S, Zhao YF. Additive manufacturing-enabled design theory and methodology: a critical review. Int J Adv Manuf Technol. 2015;80:327-342.

For Peer Review Only

List of figures

For Peer Review Only

Fig. 13 Number of Voronoi seeds estimated in relation to the target pores size for a cubic scaffold 10 mm sided with a target percentage porosity P% = 80%

Fig. 14 Pores size (measured applying the polyhedron-sphere method) of a cubic scaffold 10 mm sided, scale factors Sf = Sv = 0.75, with a target percentage porosity P% = 80%, generated with different target pores size (and therefore different number of seeds)

Fig. 15 Sample of scaffold (10x10x10 mm) with Sf= Sv = 0.75 and setting: a) number of seeds = 200 (target pores size = 2 mm), b) number of seeds = 800 (target pores size = 1 mm)

Fig. 16 Void component (pores plus connective channels) for a Voronoi scaffold with minimal scale factors (Sf = Sv = 0.25) and a) number of seeds = 8, b) number of seeds = 9

Fig. 17 Mean pores interconnection and mean channels size of a cubic scaffold 10 mm sided, scale factors Sf = Sv = 0.75, with a target percentage porosity P% = 80%, generated with different target pores size (and therefore different number of seeds)

Fig. 18 Trabecular thickness evaluation: a) Voronoi polyhedral cells scaled by Sv with the distance of the centroids of coupled faces; b) Voronoi polyhedral cells scaled by Sv with the trabecular mesh; c) the final scaffold (Sf = Sv = 0.75; number of seeds n = 12; target pores size Dp= 5 mm)

Fig. 19 Mean pores interconnection and mean channels size of a cubic scaffold 10 mm sided, scale factors Sf = Sv = 0.75, with a target percentage porosity P% = 80%, generated with different target pores size (and therefore different number of seeds)

Fig. 20 a) 3D generated Voronoi Scaffold, b) Healthy spongy bone (Marinozzi et al. 2012)

For Peer Review Only

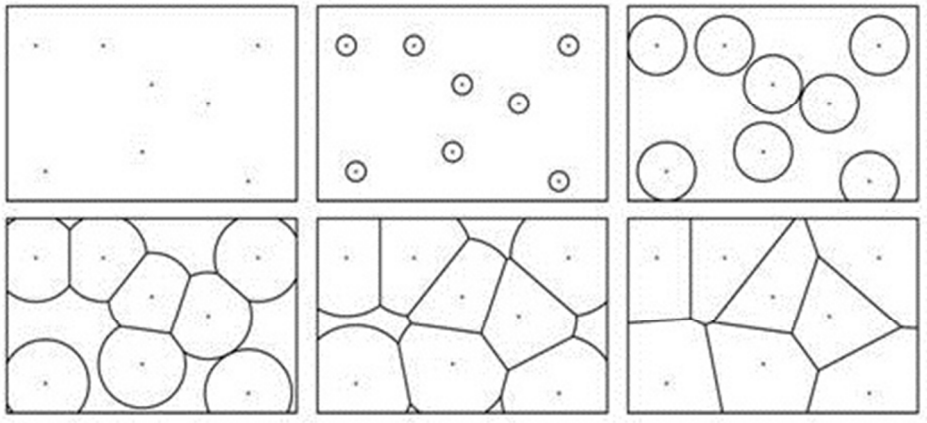

Fig. 1 Graphical representation about the formation of a 2D Voronoi diagram
123x56mm (96 x 96 DPI)

For Peer Review Only

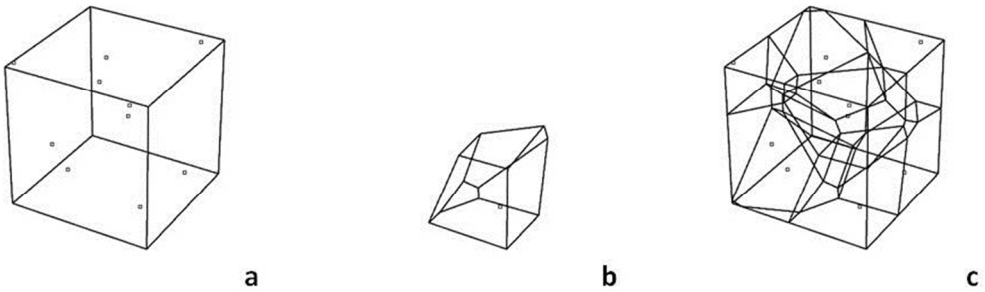

Fig.2 a) Reference cube, b) 3D Voronoi polihedron, c) Partition in 3D Voronoi polihedrons
233x72mm (96 x 96 DPI)

Peer Review Only

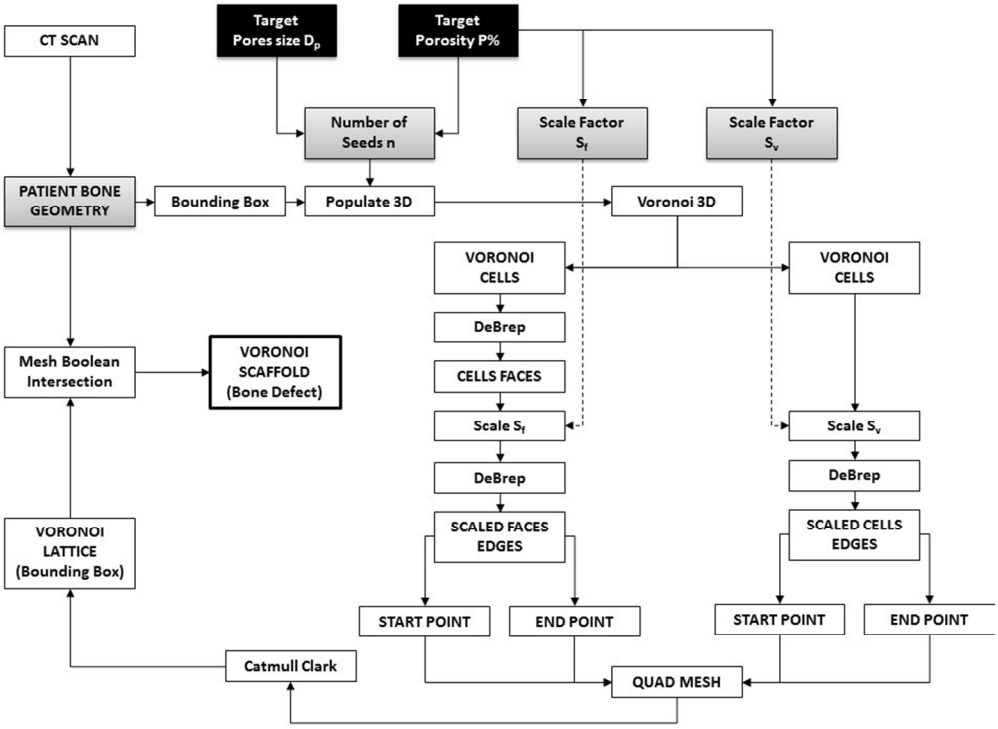

Fig. 3 Workflow for the 3D Voronoi scaffold generation
254x190mm (96 x 96 DPI)

For Review Only

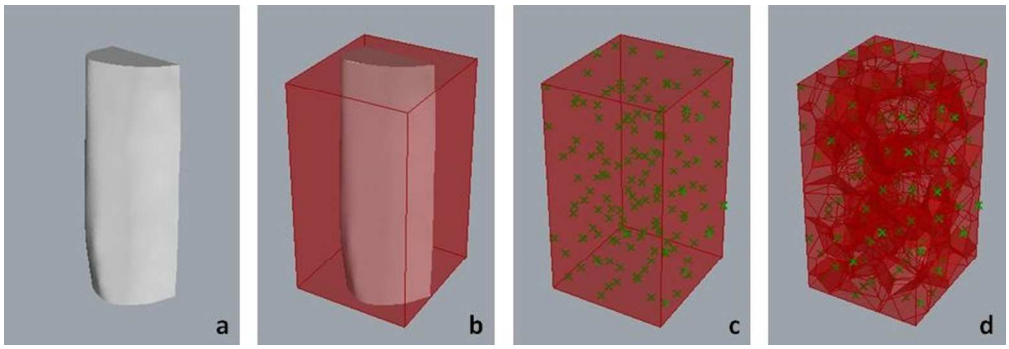

Fig. 4 Partition in Voronoi polyhedrons of the bounding box volume generated from the patient anatomy
253x86mm (96 x 96 DPI)

Peer Review Only

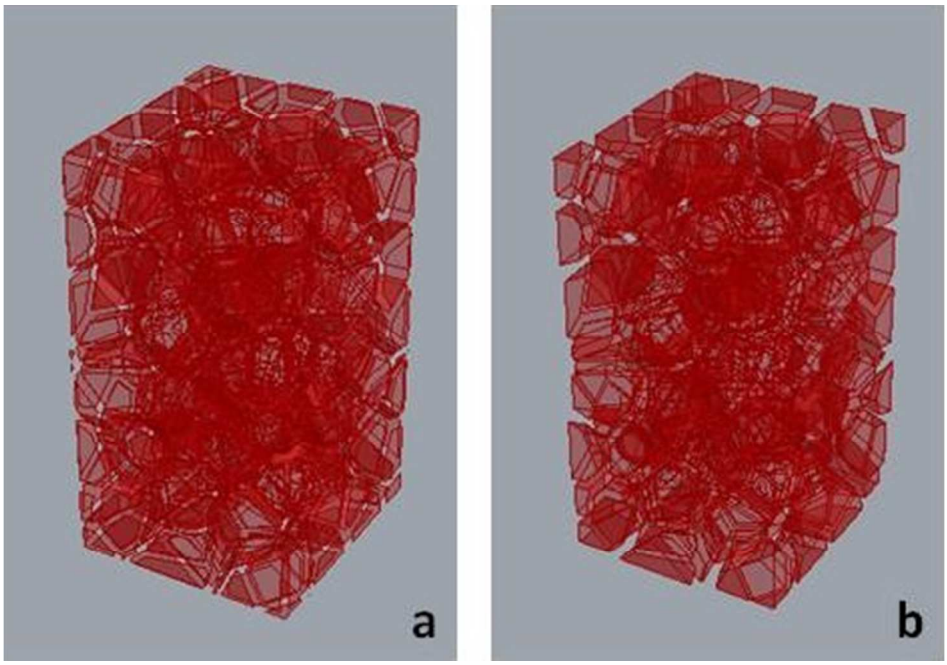

Fig. 5 a) Each face is scaled respect the face's centroid, b) each polyhedron is scaled respect the polyhedron's centroid
124x86mm (96 x 96 DPI)

For Review Only

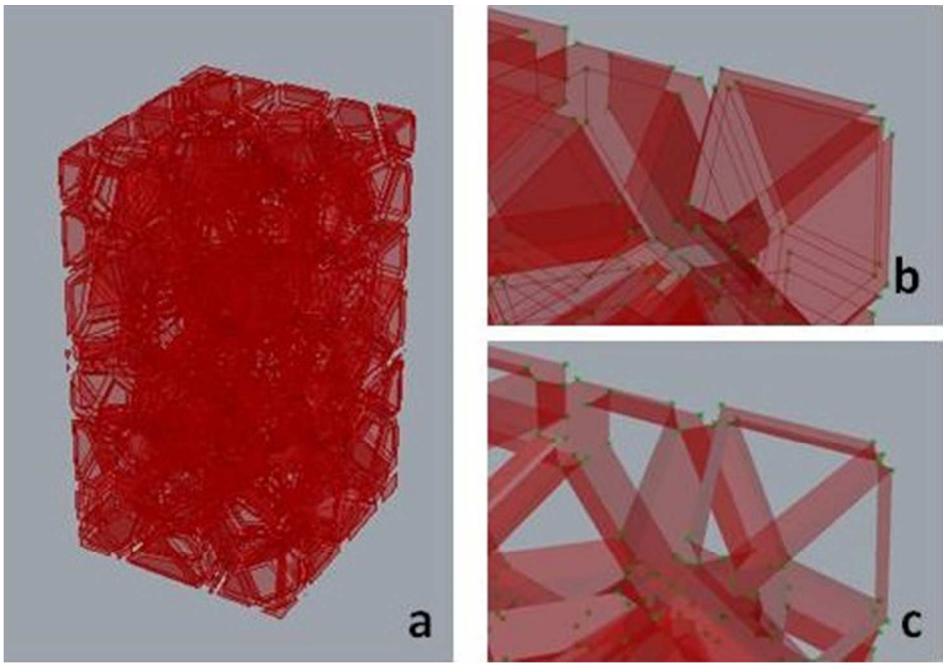

Fig. 6 a) Generation and desconstruction of faces and polihedrons, b) particular of scaled feces and polyhedrons, c) quad meshes on the edges to construct the lattice
124x86mm (96 x 96 DPI)

For Review Only

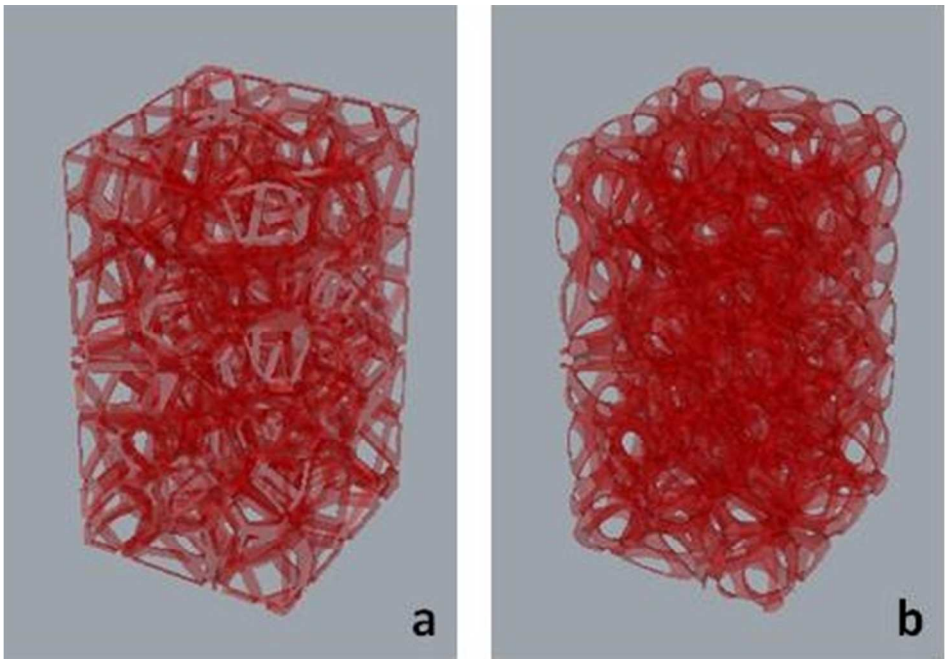

Fig. 7 a) Trabecular mesh, b) Smoothed lattice mesh after Catmull-Clark algorithm
124x86mm (96 x 96 DPI)

For Review Only

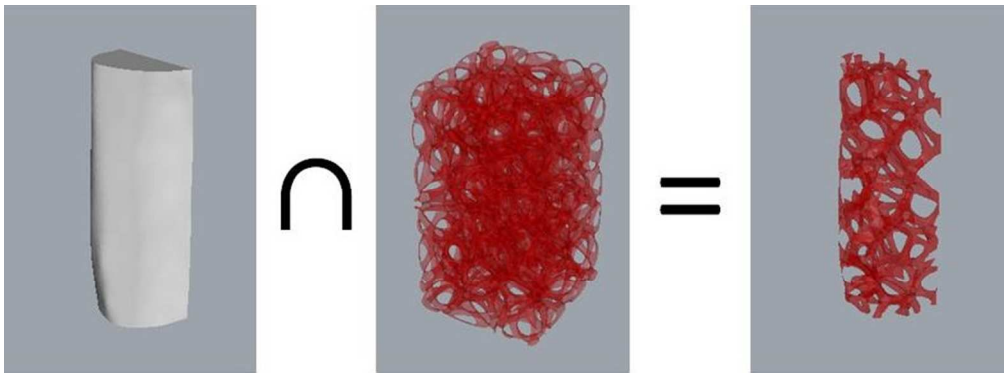

Fig. 8 Boolean intersection of the patient bone geometry and the lattices to obtain the porous scaffold
236x86mm (96 x 96 DPI)

Peer Review Only

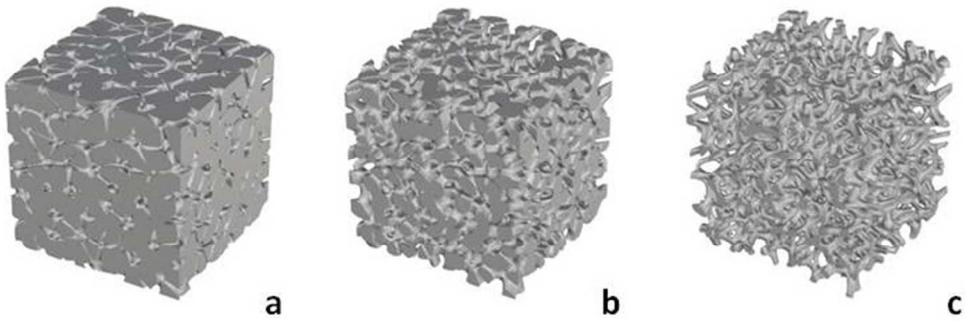

Fig. 9 Sample of scaffold (10×10×10 mm) with 500 seeds and setting: a) Sf = Sv = 0.25 (P% = 17.4), b) Sf = Sv = 0.50 (P% = 47.8), c) Sf = Sv = 0.75 (P% = 79.6)
190x65mm (96 x 96 DPI)

eer Review Only

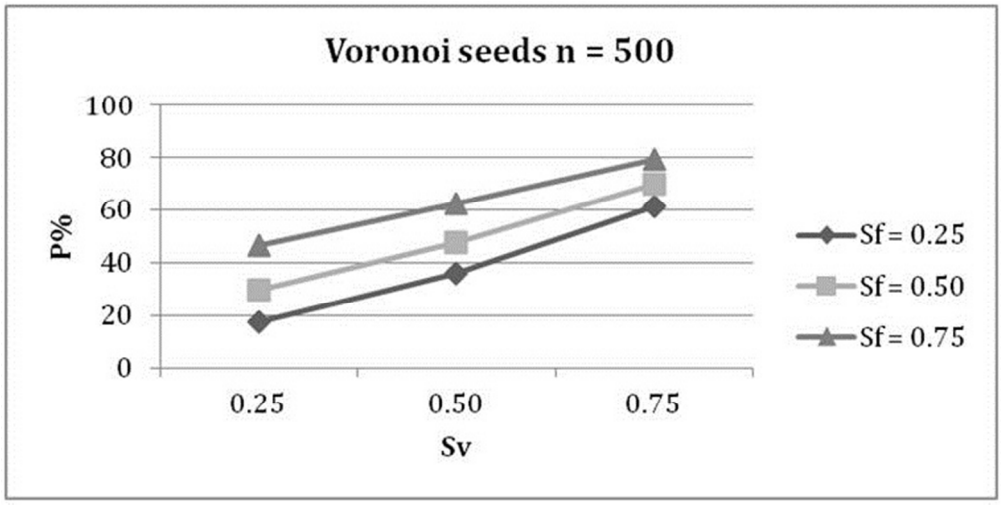

Fig. 10 Effect of the scale factors Sf and Sv on the percentage porosity of the lattice (with 500 seeds)
200x101mm (96 x 96 DPI)

For Review Only

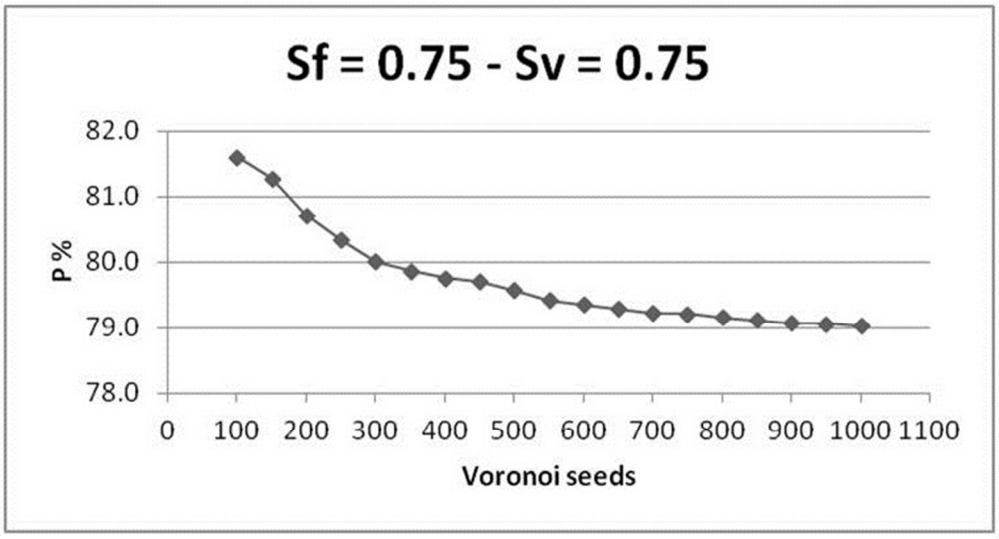

Fig. 11 Effect of the number of seeds on the percentage porosity of the scaffold (with Sf= Sv = 0.75)
201x108mm (96 x 96 DPI)

Review Only

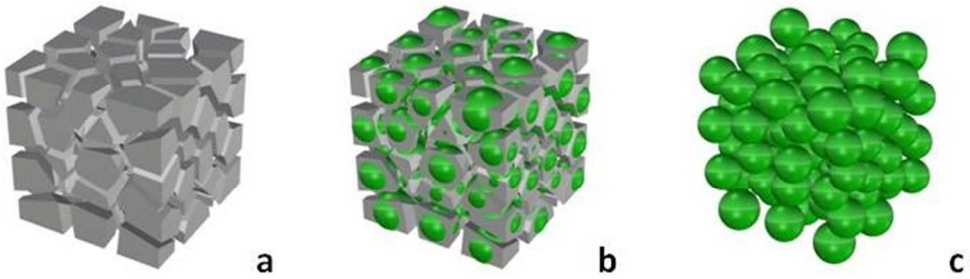

Fig. 12 Polyhedron-sphere method: a) polyhedrons scaled by Sv, b) polyhedrons scaled by Sv and corresponding spheres, c) spheres representing the pores
187x58mm (96 x 96 DPI)

Peer Review Only

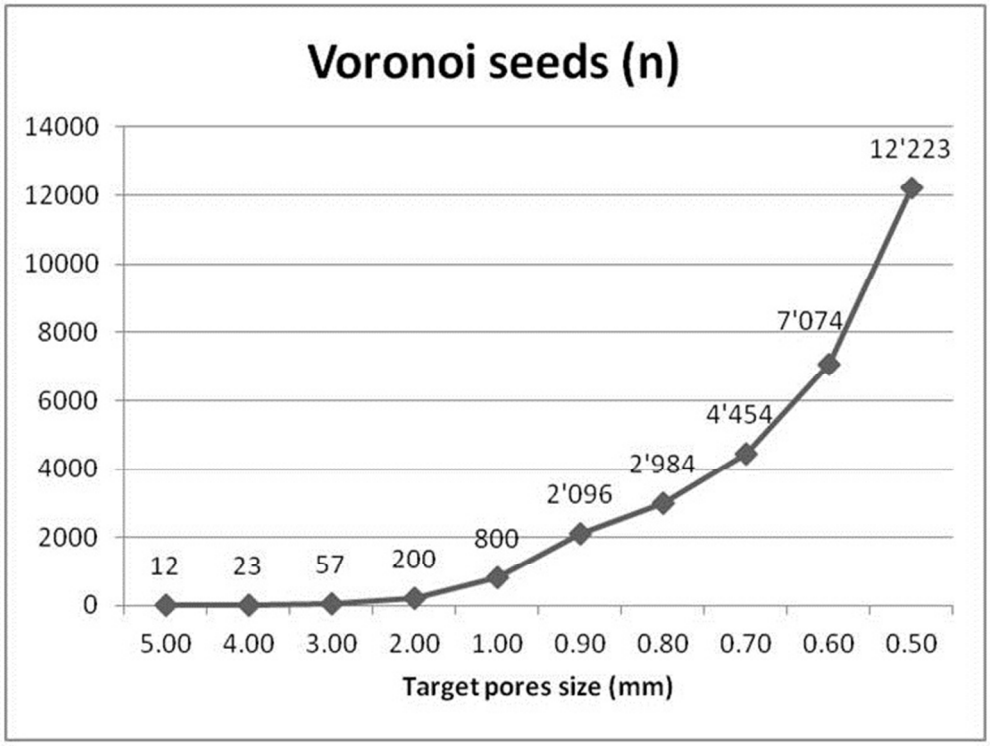

Fig. 13 Number of Voronoi seeds estimated in relation to the target pores size for a cubic scaffold 10 mm sided with a target percentage porosity P% = 80%
203x154mm (96 x 96 DPI)

For Review Only

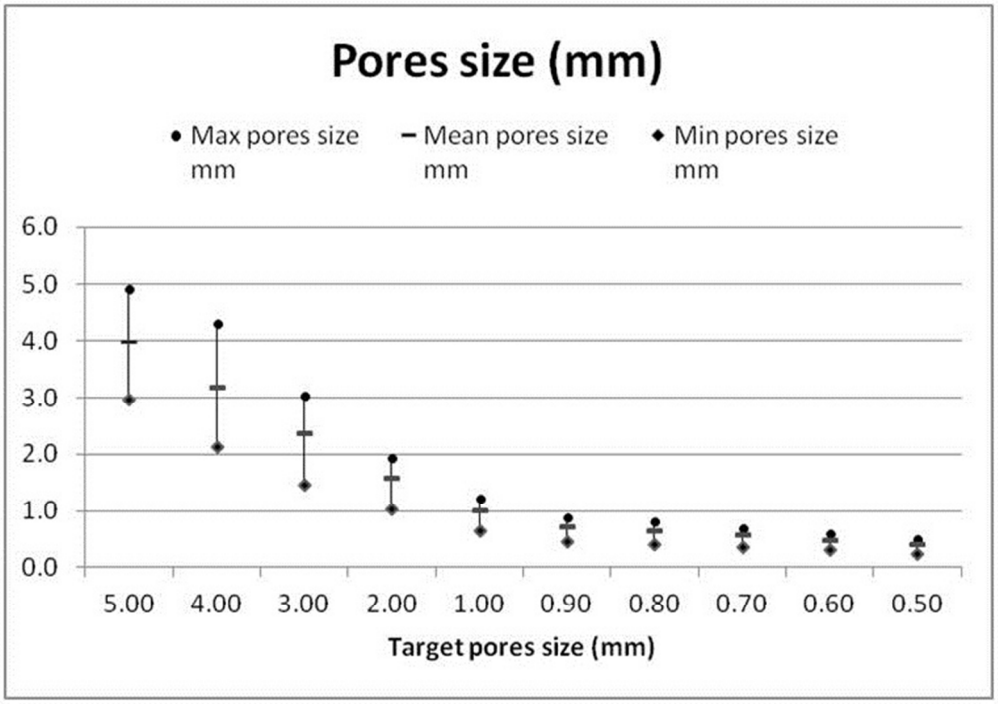

Fig. 14 Pores size (measured applying the polyhedron-sphere method) of a cubic scaffold 10 mm sided, scale factors Sf = Sv = 0.75, with a target percentage porosity P% = 80%, generated with different target pores size (and therefore different number of seeds)
201x142mm (96 x 96 DPI)

For Review Only

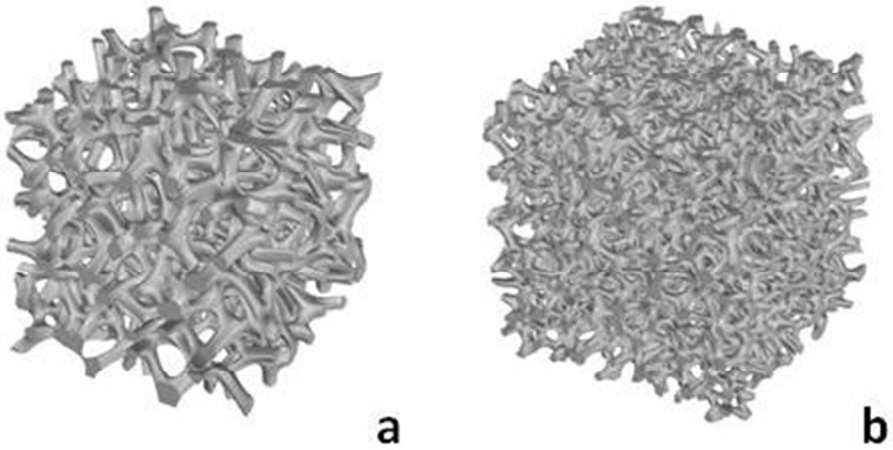

Fig. 15 Sample of scaffold (10x10x10 mm) with Sf= Sv = 0.75 and setting: a) number of seeds = 200 (target pores size = 2 mm), b) number of seeds = 800 (target pores size = 1 mm)
123x65mm (96 x 96 DPI)

For Review Only

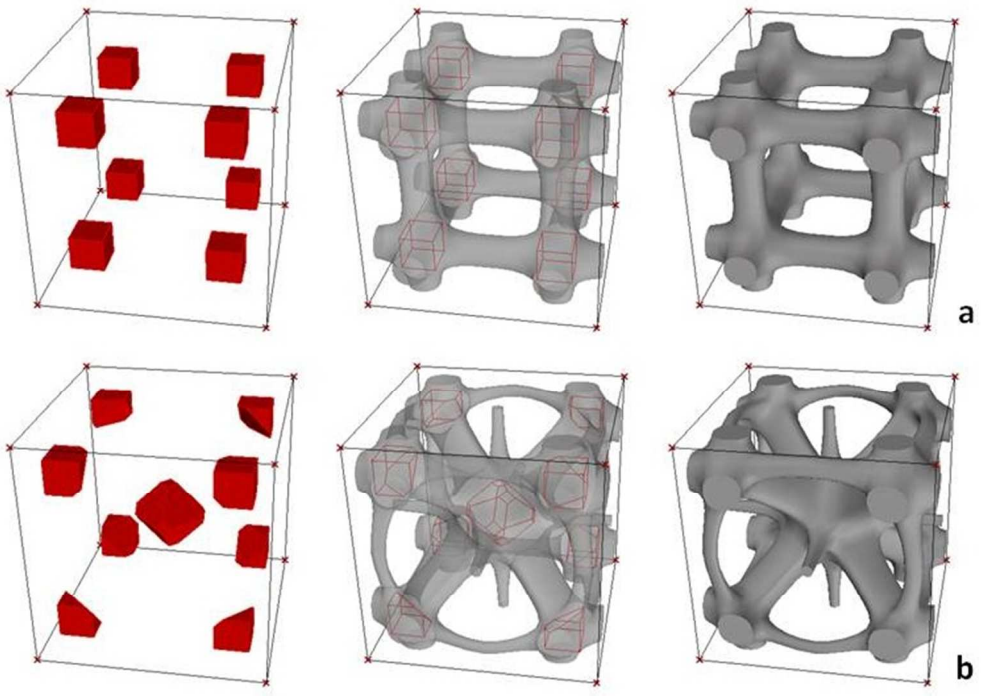

Fig. 16 Void component (pores plus connective channels) for a Voronoi scaffold with minimal scale factors (Sf = Sv = 0.25) and a) number of seeds = 8, b) number of seeds = 9
200x142mm (96 x 96 DPI)

For Review Only

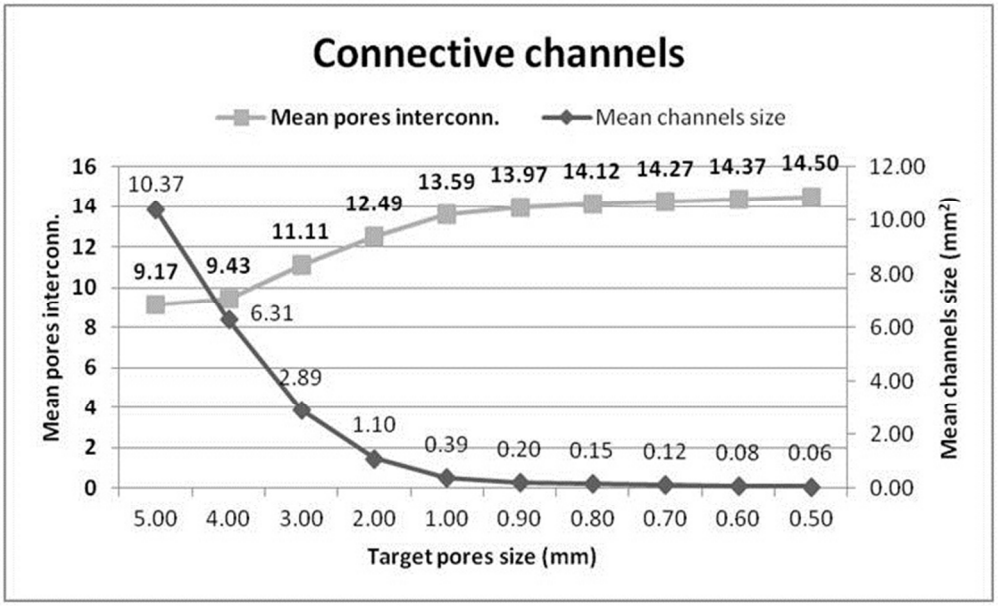

Fig. 17 Mean pores interconnection and mean channels size of a cubic scaffold 10 mm sided, scale factors Sf = Sv = 0.75, with a target percentage porosity P% = 80%, generated with different target pores size (and therefore different number of seeds)
201x123mm (96 x 96 DPI)

eview Only

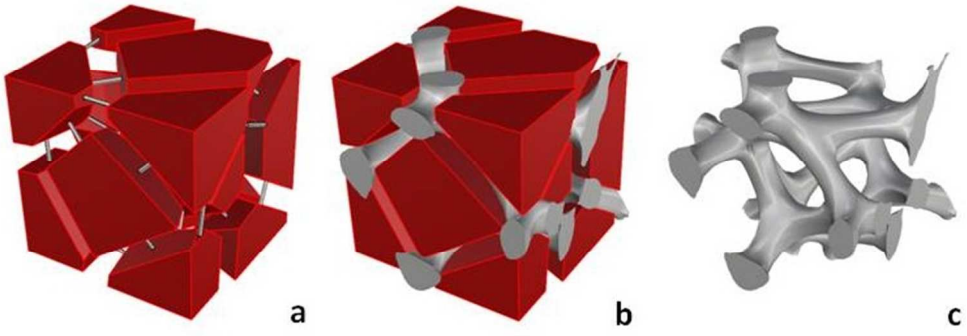

Fig. 18 Trabecular thickness evaluation: a) Voronoi polyhedral cells scaled by Sv with the distance of the centroids of coupled faces; b) Voronoi polyhedral cells scaled by Sv with the trabecular mesh; c) the final scaffold (Sf = Sv = 0.75; number of seeds n = 12; target pores size Dp= 5 mm)
203x73mm (96 x 96 DPI)

For Peer Review Only

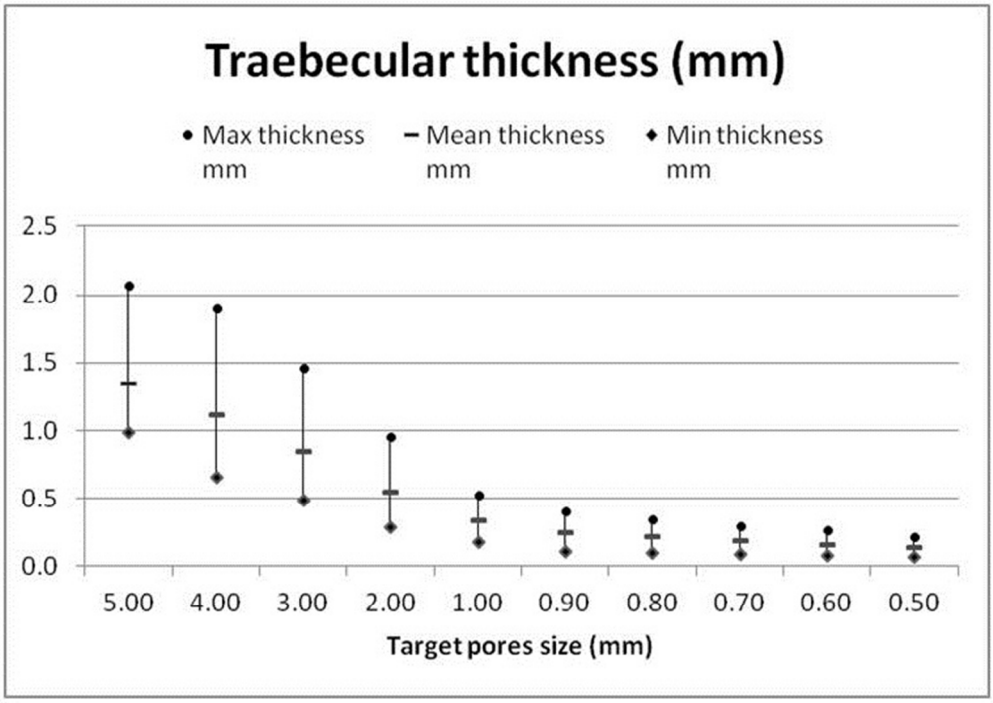

Fig. 19 Mean pores interconnection and mean channels size of a cubic scaffold 10 mm sided, scale factors Sf = Sv = 0.75, with a target percentage porosity P% = 80%, generated with different target pores size (and therefore different number of seeds)
202x142mm (96 x 96 DPI)

For Review Only

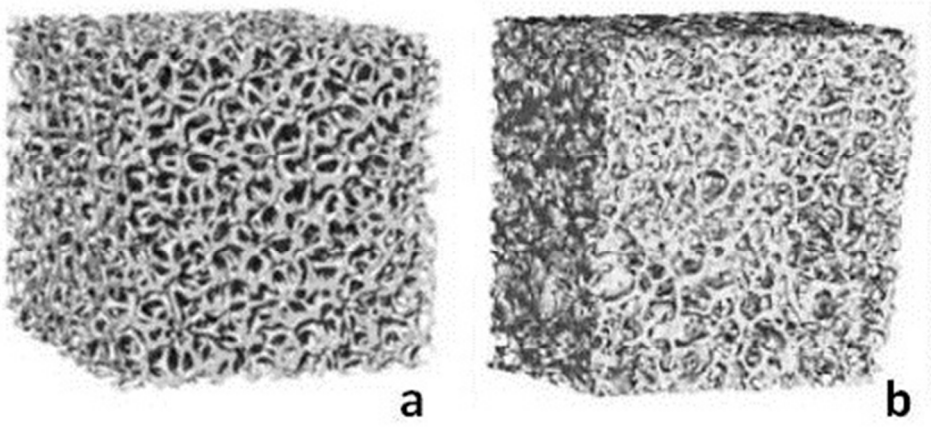

Fig. 20 a) 3D generated Voronoi Scaffold, b) Healthy spongy bone (Marinozzi et al. 2012)
125x63mm (96 x 96 DPI)

For Review Only